Contents lists available at ScienceDirect

### Journal of Organometallic Chemistry

journal homepage: www.elsevier.com/locate/jorganchem



# Amino pyridine iron(II) complexes: Characterization and catalytic application for atom transfer radical polymerization and catalytic chain transfer



Laura M. Thierer<sup>a</sup>, Sarah E. Jenny<sup>a</sup>, Vaidehi Shastri<sup>a</sup>, Marianne R. Donley<sup>a</sup>, Lindsey M. Round<sup>a</sup>, Nicholas A. Piro<sup>b</sup>, W. Scott Kassel<sup>a</sup>, Catherine L. Brown<sup>c</sup>, Timothy J. Dudley<sup>c</sup>, Deanna L. Zubris<sup>a</sup>,\*

- <sup>a</sup> Department of Chemistry, Villanova University, Villanova, PA 19085, United States
- <sup>b</sup> Department of Chemistry and Biochemistry, Albright College, Reading, PA 19604, United States
- <sup>c</sup> Math, Science and Technology Department, University of Minnesota Crookston, 2900 University Avenue, Crookston, MN 56716, United States

#### ARTICLE INFO

#### Article history: Received 19 May 2020 Revised 20 July 2020 Accepted 21 July 2020 Available online 24 July 2020

Keywords: Amino-pyridine ligand Iron X-ray structure ATRP

#### ABSTRACT

The amino-pyridine ligand scaffold has achieved widespread use for base metal catalysis. Atom Transfer Radical Polymerization (ATRP) is one realm where base metals have achieved success in catalysis, in particular copper and iron. Herein, the synthesis and characterization of two amino-pyridine iron(II) complexes is described where the amino carbon substitution is the point of differentiation. We hypothesized that a sterically hindered, electron rich t-butyl substituent in this position might improve the propensity of said complex to achieve ATRP since inductive electron donation from the t-butyl group may improve catalyst activity and shift the ATRP equilibrium towards the active polymer species and corresponding Fe(III) complex. Dimeric 1 and 2 ([2-[(2,6-Me\_2-C\_6H\_3)NHCH(R)]C\_5H\_4N]FeCl\_2)<sub>2</sub> (R = t-butyl or ethyl, respectively) were identified by single crystal X-ray diffraction. Both complexes favor a high-spin iron(II) state, as evidenced by Evans NMR magnetic susceptibility measurements and suggested by gas-phase computations at the M06-L level of theory. Complexes 1 and 2 catalyze styrene polymerization at elevated temperatures (120 °C) and polymerization data suggests that ATRP operates and catalytic chain transfer (CCT) competes at extended reaction times. Complex 1 with its t-butyl substituted amino carbon displays a slightly higher ATRP activity as compared to 2 [ $k_{obs}(1) = 0.31 \ h^{-1}$ ;  $k_{obs}(2) = 0.10 \ h^{-1}$ ], suggesting the importance of ligand optimization for future iron ATRP catalyst development.

© 2020 Elsevier B.V. All rights reserved.

#### 1. Introduction

Base metal homogeneous catalysis is a fertile research area that is growing rapidly as chemists embrace this approach to minimize costs and move into new catalytic space [1-4]. Atom transfer radical polymerization (ATRP) is a catalytic application where base metal catalysts have played a major role at both the inception of the field and development of catalysis [5-14]. Base metal copper [15] and precious metal ruthenium [16] were both part of ATRP's discovery in the mid-1990's and have continued to dominate this chemistry. The homogeneous metal catalyst serves as a halogen atom donor and acceptor towards the active and dormant polymer species, respectively, that are necessary for the equilibrium

that characterizes ATRP (Fig. 1). Catalytic chain transfer (CCT) is a common competing mechanism that operates concurrently with ATRP, leading to premature polymer chain termination with an alkene polymer end group and polymer molecular weights that are lower than expected  $M_n$ (theoretical) values for a pure ATRP process (Fig. 1) [17].

Imino-pyridine and amino-pyridine ligands are two examples of nitrogenous ligands that have been employed widely in base metal catalysis, with the benefit of readily tunable N-aryl or N-alkyl substituents. Installation of substituents at other positions of the ligand, such as the 6-position of the pyridyl ring ( $R_2$ ) or the imino/amino carbon position ( $R_1/R_3$ ), typically requires additional synthetic steps [18] and hence their impact on polymerization metrics such as catalyst activity, polymer molecular weight, and polymer dispersity are not fully understood for coordination polymerization or ATRP. Our group [19] and others [20-22] have incorporated sterically bulky imino/amino carbon

<sup>\*</sup> Corresponding Author. E-mail address: deanna.zubris@villanova.edu (D.L. Zubris).

Fig. 1. ATRP equilibrium between active and dormant polymer chains mediated by a metal complex in oxidized and reduced form, respectively. CCT leads to polymer chain termination that may occur via direct hydrogen atom transfer.

Ar 
$$R_1 = Et$$
  $R_1 = Et$   $R_1 = Et$   $R_2 = Et$   $R_3 = Et$   $R_3 = Et$   $R_4 = Et$   $R_5 = Et$   $R_1 = Et$   $R_2 = Et$   $R_3 = Et$   $R_4 = Et$   $R_4 = Et$   $R_5 = Et$   $R_5 = Et$   $R_6 = Et$   $R_7 = Et$   $R_8 = Et$   $R_1 = Et$   $R_1 = Et$   $R_2 = Et$   $R_1 = Et$   $R_2 = Et$   $R_3 = Et$   $R_4 = Et$   $R_1 = Et$   $R_2 = Et$   $R_3 = Et$   $R_4 = Et$   $R_4 = Et$   $R_5 = Et$   $R_6 = Et$   $R_7 = Et$   $R_8 = Et$   $R_8 = Et$   $R_8 = Et$   $R_8 = Et$   $R_9 = E$   $R_9 = Et$   $R_9 = E$ 

Chart 1. Reported imino- and amino-pyridine Ni(II) complexes where variations in R<sub>1</sub> and R<sub>3</sub> were explored. All substituent options presented.

substituents  $(R_1/R_3)$  in nickel(II) bromide catalysts for coordination polymerization of ethylene, yielding improvements in catalyst activity, polymer molecular weight and dispersity when compared to the more typical option of  $R_1=H$  or Me and  $R_3=H$  (Chart 1).

Base metal iron is an attractive metal for ATRP due to its high natural abundance, low cost, and biocompatibility. Homogeneous iron catalysts have achieved success for ATRP as first reported in 1997 [23-24], and more recently described by excellent reviews [25-27], yet ligand design principles are not fully developed for this chemistry. Four-coordinate, high-spin iron(II) complexes with electron-donating nitrogenous ligands have been successful (selected examples presented in Chart 2, blue font) [28-30], though they have not achieved the high activities and low catalyst loadings observed for state-of-the art copper catalysts [31]. Gibson's tridentate salicylaldiminato iron(II) catalysts [32], Grubbs' bis(N-heterocyclic carbene) iron(II) catalysts [33], Shaver's amine bis(phenolate) iron(III) complexes [34-35] and Garden and Shaver's half salen iron(III) complexes [36] further demonstrate the scope of ligand substitution patterns that favor ATRP (or reverse ATRP for the Fe(III) examples). Despite these examples, many ATRP catalysts are prepared in-situ, adding to the challenge of discerning ligand design principles for ATRP when the nature of the operating iron complexes is not the focus of investigation.

Since amino-pyridine ligands are most often synthesized through reduction of the corresponding imino-pyridines, it is useful to reflect on the scope of reported imino- and amino-pyridine iron(II) complexes to help extend this chemistry in new directions. Reported examples of imino- and amino-pyridine Fe(II) catalysts appear in Chart 2; aside from Gibson's report [28] for ATRP catalysis of styrene and methyl methacrylate, others have used these

imino- [37-40] and amino- [41] pyridine Fe(II) catalysts for coordination polymerization of isoprene.

Herein, we describe the synthesis and characterization of two amino-pyridine iron(II) complexes where the amino-carbon substituent is varied and describe how this subtle difference correlates with changes in styrene polymerization outcomes. Computational analysis helps us explore the energetics of the ATRP and CCT equilibria for our catalysts. These experimental and computational results help inform our ongoing pursuit of rationally designed iron ATRP catalysts.

#### 2. Results and discussion

#### 2.1. Synthesis and characterization of iron(II) complexes

Metalation of the alkyl-substituted amino-pyridine ligands, [2- $[(2,6-Me_2-C_6H_3)NHC(R)]C_5H_4N]$  (where R=t-Bu or Et), with FeCl<sub>2</sub>(THF)<sub>15</sub> in toluene solvent gives complexes with the desired one to one ratio of chelating ligand to iron (Fig. 2). Complex 1 (R = t-Bu) was isolated as a tan solid with a diagnostic  $\nu(N-H)$ IR stretching frequency at 3340 cm $^{-1}$ ; complex 2 (R = Et) was isolated as a tan solid with a diagnostic  $\nu(N-H)$  IR stretching frequency of 3326 cm<sup>-1</sup>; both of these stretching frequencies are lower in energy than the corresponding uncomplexed ligand N-H stretching frequencies, (3386 and 3414 cm<sup>-1</sup> for R = t-Bu and 3362 cm<sup>-1</sup> for R = Et). Complexes 1 and 2 were tested by Evans' NMR method for magnetic susceptibility [42] and the data supports a high spin Fe(II) designation for both 1 and 2: complex 1  $\mu_{\rm eff}$  = 5.71 B.M., and complex **2**  $\mu_{\rm eff}$  = 5.51 B.M.. Complexes **1** and 2 were also examined by <sup>1</sup>H NMR (CD<sub>2</sub>Cl<sub>2</sub>) and spectra are consistent with their paramagnetic nature (see Supplemental Material, Figures S6 and S7).

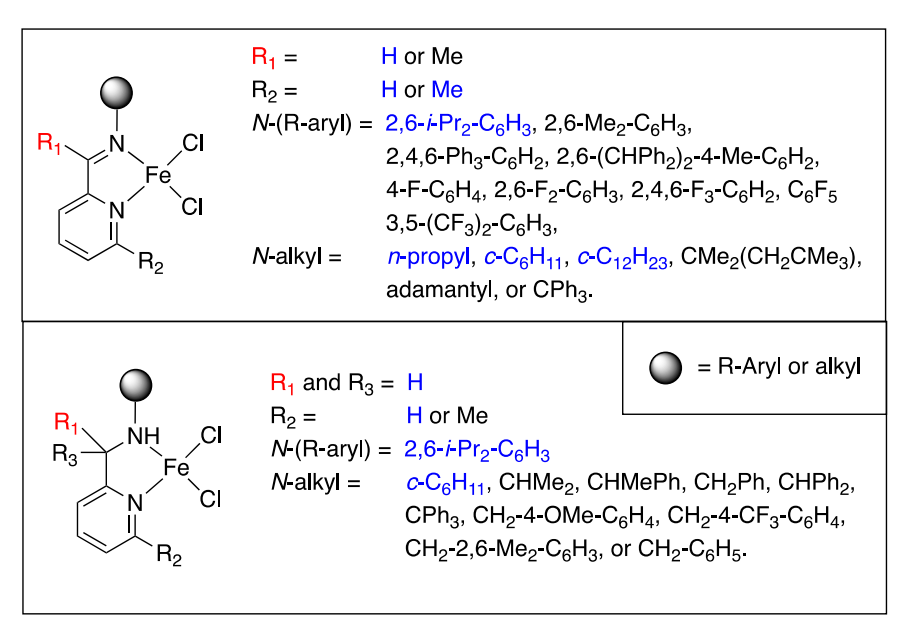


Chart 2. Reported imino- and amino-pyridine Fe(II) complexes. All substituent options presented. Examples in blue font were tested by Gibson and coworkers for ATRP catalysis of styrene and methyl methacrylate [28].

**Fig. 2.** Metalation of amino-pyridine ligands in toluene yields {[2-[(2,6-Me<sub>2</sub>- $C_6H_3)NHC(R)]-C_5H_4N]FeCl<sub>2</sub>}<sub>2</sub> (<math>R = t$ -Bu 1; R = Et 2). Conditions for 1: 80 °C, 18 h then 100 °C, 23 h; conditions for 2: 80 °C, 21 h.

Single crystals of **1** and **2** were evaluated by X-ray diffraction studies and revealed dimeric solid-state structures. Each Fe(II) atom adopts a distorted trigonal bipyramid geometry with a  $\tau_5$  value of 0.69 for **1** and a  $\tau_5$  value of 0.82 for **2** (Fig. 3) [43]. Crystals of **1** were obtained by slow cooling of an acetonitrile solution to -30 °C, and crystals of **2** were obtained by vapor diffusion of pentane into a dichloromethane solution at room temperature. Other crystallization conditions, including slow evaporation from a tetrahydrofuran solution and vapor diffusion of pentane into a

dichloromethane solution, produced single crystals of **1** with the same unit cell as above.

A dimeric structure can be commonplace for an aminopyridine ligand scaffold, as reported by Gao and Wu for a related nickel(II) example  $\{[2-[(2,6-i-Pr_2-C_6H_3)NHC(Me)H]C_5H_4N]NiBr_2\}_2$ [21] and J.-T. Chen for another nickel(II) example {[(2,6-i-Pr<sub>2</sub>- $C_6H_3$ )NHCH<sub>2</sub>] $C_5H_4$ N]NiBr<sub>2</sub>}<sub>2</sub> [22]. We anticipate the dimeric structure is in equilibrium with a closely related monomeric structure in solution, especially under polymerization conditions at elevated temperature. X. Wang, Q. Wang, and coworkers [41] also made this argument based on the observation of multiple crystal structures of amino-pyridine iron(II) chloride complexes with only subtle ligand modifications; for example,  $\{2-Me,6-[(CHPh_2)NCH_2]C_5H_4N\}FeCl_2$  and  $\{2-Me,6-(CHPh_2)NCH_2\}C_5H_4N\}FeCl_2$  $[(CH_2Ph)NCH_2]C_5H_4N \} FeCl_2 \quad crystallized \quad as \quad monomers, \quad \{[2 [(CHMePh)NCH_2]C_5H_4N]FeCl_2\}_2$  crystallized as a dimer, and  $\{[2-[(c-C_6H_{11})NCH_2]C_5H_4N]FeCl_2\}_3$  crystallized as a trimer with two terminal iron atoms, one central iron atom, and bridging chloride ligands. All four of these iron complexes are competent for isoprene polymerization upon activation with MAO cocatalyst at room temperature, suggesting potential equilibration of these monomeric, dimeric, and trimeric forms under reaction conditions.

Bond angles and distances are typical in complexes 1 and 2, with the t-butyl substituent influencing the  $N_{pyr}$ -Fe- $N_{amine}$  bite an-

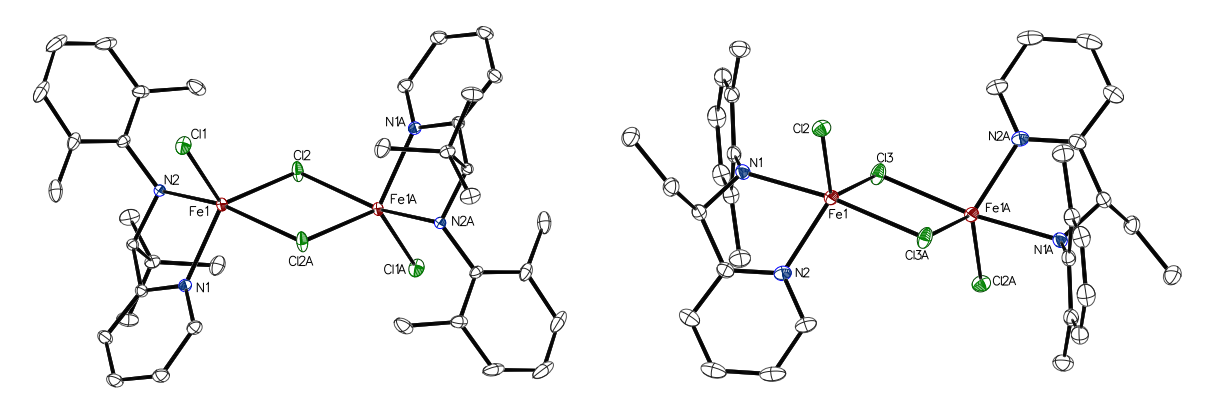


Fig. 3. ORTEP diagrams for  $\{[2-[(2,6-Me_2-C_6H_3)NHC(R)]C_5H_4N]FeCl_2\}_2$  (left, R=t-Bu 1; right, R=t 2). Thermal ellipsoids are shown at the 50% probability level.

Fig. 4. Styrene ATRP screening conditions for catalysts 1 and 2 [Fe]: [styrene]: [Fe]: [1-phenylethyl chloride] = 300: 1.0: 1.0: 1.0: 1.0: 1.0 °C, 10-11 h.

Table 1
Selected bond distances (Å) and angles (deg) for 1 and 2.

	Bond distances (Å) and angles (deg)		
	C-N (Å)	N-Fe-N (deg)	
1	1.494	75.89	
2	1.493	77.53	
	Fe-N <sub>pyridine</sub> (Å)	Fe-N <sub>amine</sub> (Å)	
1	2.1168(7)	2.3176(6)	
2	2.1097(10)	2.2945(9)	

gle to a larger extent than other bond angles and distances (bite angle of 75.89° for *t*-butyl substituted **1** versus 77.53° for ethyl substituted **2**). The C-N amine bond lengths for both **1** and **2** are consistent with C-N single bond character as anticipated, and the Fe-N<sub>pyr</sub> bond lengths are shorter than the Fe-N<sub>amine</sub> bond lengths, consistent with the relative donor ability of these nitrogen atoms. Further, the Fe-N<sub>amine</sub> bond distances for **1** and **2** are up to 0.18 Å longer than those reported by X. Wang, Q. Wang, and coworkers [41] for amino-pyridine iron(II) chloride complexes with *N*-alkyl substituents, suggesting a slightly weaker amino-*N* donor interaction for **1** and **2** as may be expected for an *N*-aryl substituted donor atom. Selected bond distances and angles for **1** and **2** are given in Table **1**.

#### 2.2. Styrene polymerization

Complexes **1** and **2** were tested for bulk polymerization of styrene at 120 °C using 1-phenylethyl chloride as initiator (In) for a reaction time of 10–11 h and terminated based on reaction mixture viscosity (Fig. 4). Elevated reaction temperatures can be common in this field, particularly for bulk styrene polymerizations [26]. Aliquots were removed at regular intervals, quenched by passage over basic alumina, eluted with chloroform-*d*, and then analyzed

by  $^1\text{H}$  NMR spectroscopy to calculate percent monomer conversion. This monomer conversion data was plotted versus time (see Fig. 5), and used to prepare semilogarithmic plots of  $ln([M]_0/[M])$  versus time (see Fig. 6). Given the pseudo first order conditions of ATRP reactions, both of these plots are expected to be linear under an operative ATRP mechanism.

Controlled radical polymerization is suggested by the linearity of the data presented in Figs. 5 and 6, yet one cannot distinguish ATRP versus CCT behavior from these plots alone (vide infra). Others have reported that the ATRP mechanism can operate alongside competing CCT, and turned to polymer end-group analysis and examination of  $M_n$  (theoretical) values to probe the preferred polymerization mechanism for a given family of catalysts [17,44-45]. Fig. 6 may be used to calculate experimental polymerization rate constants,  $k_{obs}$ , for catalysts 1 and 2. Catalyst 1 presents a markedly faster polymerization rate than catalyst **2** [ $k_{obs}(\mathbf{1}) = 0.31$  $h^{-1}$ ;  $k_{obs}(\mathbf{2}) = 0.10 \ h^{-1}$ ]. This data suggests that catalyst **1**, with its t-butyl amino carbon substituent, helps stabilize the Fe(III) form of the complex thereby favoring the left side of the ATRP propagation equilibrium (Fig. 1). Catalyst 1 may also accommodate the three chloride ligands of the Fe(III) complex more easily than catalyst 2 due to its smaller Npyr-Fe-Namine bite angle. The rate constants for catalysts 1 and 2 are on the same order of magnitude as the family of  $\alpha$ -diimine iron(II) and iron(III) complexes reported by Gibson and Shaver, with  $\{Cy-N=C(p-NMe_2-Ph)-C(p-NMe_2-Ph)=N-Ph\}$ Cy} including an electron donating dimethylamino substituent that is the most active of the series with a  $k_{obs}$  value of 0.72  $h^{-1}$ [44]. Catalysts 1 and 2 are not as active for styrene polymerization as Shaver's most active amine bis(phenolate) iron(III) complexes [34-35] which are the fastest reported iron complexes to date for styrene ATRP with  $k_{obs}$  values of 1.02  $h^{-1}$  and  $2.20 \ h^{-1}$  for their two fastest examples.

Polymer molecular weight and dispersity ( $\mathcal{D}$ ) data also lend insight for the operating polymerization mechanism. The aliquots

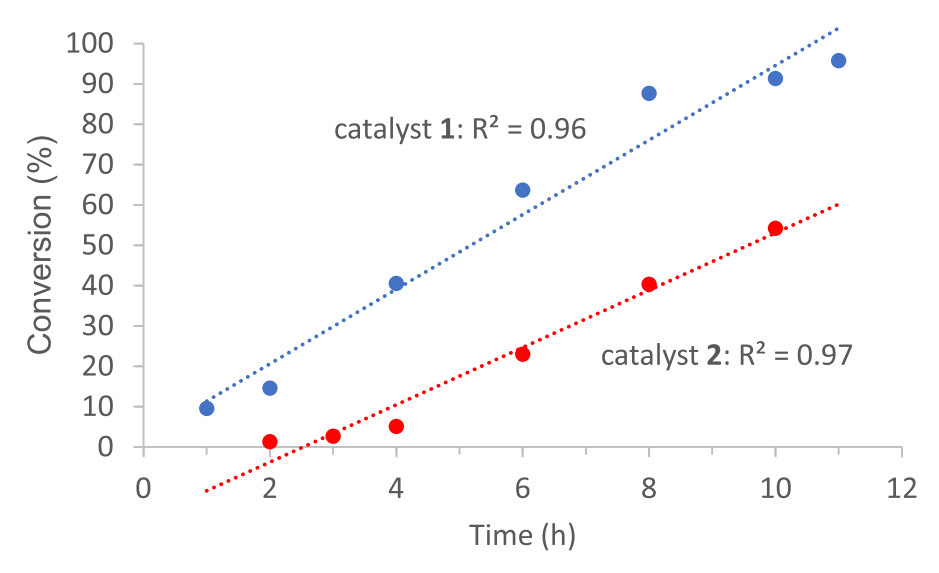


Fig. 5. Plot of conversion (%) vs. time (h) for 1 and 2.

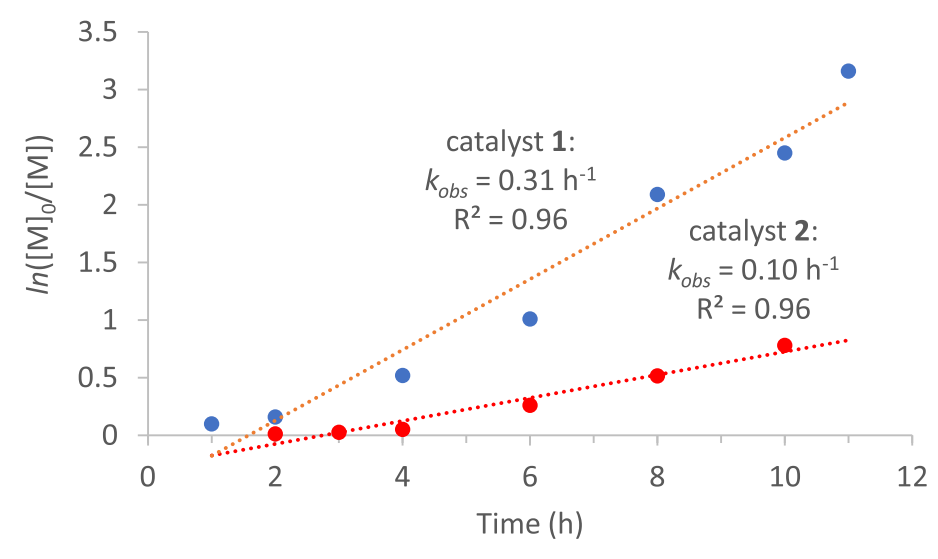


Fig. 6. Kinetic plot for styrene polymerization:  $ln([M]_0/[M])$  vs. time (h) for 1 and 2.

Table 2
Styrene ATRP screening for catalysts 1 and 2.a

Entry	Complex	Time (h)	Conv. (%) b	$M_{n, th}$ c	$M_{n, GPC}$	Đ
1	1	2	14.6	4710	4250	1.55
2		4	40.6	13,110	4930	1.85
3		8	87.7	28,310	3940	2.48
4		10	91.3	29,470	3630	2.52
5	2	2	1.3	400	2750	1.56
6		4	5.1	1540	3360	1.82
7		8	40.3	12,180	4740	2.10

<sup>a</sup>Conditions: [styrene]:[Fe]:[1-phenylethyl chloride] = 300 : 1.0 : 1.0, 120 °C.

used for <sup>1</sup>H NMR spectroscopy, as described above, were also used to conduct GPC analysis of precipitated polymer to measure  $M_n$  and D for representative samples. Percent monomer conversion,  $M_n(GPC)$ ,  $M_n$  (theoretical), and D values at representative time points are reported in Table 2. Styrene oligomers are formed by both catalysts, with D values that exceed the ideal value of 1.0 for living polymerization. For catalyst 1,  $M_n$  values slowly decrease over time: slowly increasing D values may account for this phenomenon, as supported by GPC traces that approach a bimodal form with a growing low-molecular weight fraction concurrent with the slowing of polymer growth for the higher molecular weight chains (see Supplemental Material, Figure S10). This observation suggests the higher rate constant,  $k_{obs}$ , for catalyst 1 is accompanied by some loss of polymerization control. Catalyst 2 operates more slowly, as reflected by its modest % conversion values, and both  $M_n$  and D slowly increase over time. GPC traces for these polymer samples (Figure S10) also reflect a low-molecular weight fraction though it appears less pronounced than for polymers formed by catalyst **1**. Lastly, values for  $M_n(GPC)$  and  $M_n$  (theoretical) diverge as a function of time, consistent with a transition from an ATRP mechanism at early time points to a CCT mechanism at later time points. Overall, the  $M_n$  and D data for representative samples suggests competing polymerization mechanisms.

Under the reaction conditions described in Fig. 4, propagating polystyrene may terminate through a variety of means as revealed by NMR spectroscopic analysis of the polymer end groups (see Fig. 7). ATRP gives halide-terminated polymer chain ends as shown in Fig. 7; a ClCH(Ph)CH<sub>2</sub>-(polymer) chain end has a diagnostic pro-

Fig. 7. Diagnostic protons for CCT and ATRP end groups.

ton at 4.35 ppm (H<sub>d</sub>) [36]. Catalytic chain transfer (CCT) often competes with ATRP and theoretical models suggest it occurs via direct H-atom transfer from the growing polymer chain to the metal [17], yielding a L<sub>n</sub>FeCl<sub>2</sub>H species and alkene terminated polymer chain end. The  $H_2C=CH(Ph)CH_2$ -(polymer) chain end has characteristic doublets at 5.27 and 5.78 ppm (Ha and Hb, for the alkene protons, and a signal located between 6.05 and 6.35 ppm for the vinylidene C-H (H<sub>c</sub>) [36,46]. Similarly, an alkene terminated chain end with a phenyl substituent at the terminus, H(Ph)C=CHC(Ph)HCH2-(polymer) has a characteristic allylic signal at 4.12 ppm (H<sub>e</sub>). Other polymerization mechanisms such as organometallic mediated radical polymerization (OMRP) [47-48], catalyzed radical termination (CRT), and reductive radical termination (RRT) have also come to light more recently, yielding saturated chain ends derived from the reactive radical [49]. And finally, conventional free-radical polymerization may terminate via combination (doubling the observed polymer molecular weight and leaving both end groups with the functionality introduced through initiation) or disproportionation (providing one alkyl and one alkene terminated chain end) although combination is strongly favored over disproportionation at higher temperatures [50]. Atactic polystyrene is expected for radical polymerization mechanisms such as ATRP and CCT, as described elsewhere [51].

End group analysis of isolated polymer samples produced by catalysts  ${\bf 1}$  and  ${\bf 2}$  reveals evidence for both ATRP and CCT polymerization mechanisms.  $^1H$  NMR spectra of polymer samples from the 8-hour aliquot are presented in the Supplemental Material (Figures S11 and S12, respectively). For polystyrene generated by catalyst  ${\bf 1}$ , protons that correspond to a CICH(Ph)CH $_2$  ATRP chain end (H $_d$ ),  $H_2$ C=CH(Ph)CH $_2$  CCT chain end (H $_a$  and H $_b$ ), CCT vinylidene signal (H $_c$ ), and CCT allylic signal (H $_e$ ) are all detected. For polystyrene

<sup>&</sup>lt;sup>b</sup>Conversion (%) determined by <sup>1</sup>H NMR spectroscopy.

 $<sup>{}^{</sup>c}M_{n, th} = ([M]_0/[I]_0) \times MW \text{ (styrene)} \times \text{conversion.}$ 

generated by catalyst  ${\bf 2}$ , protons that correspond to a CICH(Ph)CH $_2$  ATRP chain end (H $_d$ ), CCT vinylidene signal (H $_c$ ), and CCT allylic signal (H $_e$ ) are detected. At this later phase in the polymerization, CCT is more prominent than at earlier time points (see Supplemental Material, Figure S13). There are a large number of peaks in this region of the spectrum due to the oligomeric, atactic nature of these polystyrene samples; representing many subtly distinct chemical shift environments.

## 2.3. Computational analysis of iron complexes and competing polymerization mechanisms

Poli and Shaver published an elegant study in 2014 describing the power of DFT methods to evaluate the balance between ATRP, CCT, and OMRP (Organometallic Mediated Radical Polymerization) mechanisms for  $\alpha$ -diimine iron(II) catalysts [17]. Earlier work by Gibson and Shaver suggested that ligand substituents influenced the spin state of  $\alpha$ -diimine iron(III) (reverse ATRP) catalysts, and that iron(III) complexes with intermediate spin (quartet) favored CCT while iron(III) complexes with high spin (sextet) favored ATRP [29-30,52]. The 2014 Poli and Shaver study [17] revises this claim and suggests that iron complex spin state does not dictate polymerization mechanistic preferences. Instead, they propose the barrier to ATRP radical propagation is ligand-independent for  $\alpha$ -diimine iron(II) complexes and the influence the ligand has on the relative thermodynamics of ATRP, CCT, and OMRP dictates which of these mechanisms is favored under experimental conditions

Accordingly, we completed geometry optimizations and gasphase energy calculations on the monomeric forms of iron(II) complexes **1** and **2** (**3a** and **3b** from Fig. 8, respectively) using DFT (M06-L) with a double-zeta quality basis set. In both cases, gasphase M06-L electronic energy calculations predict the high spin quintet state is the ground state; the intermediate spin triplet state is 26.0 kcal/mol higher in energy for **3a** and 25.2 kcal/mol higher in energy for **3b** (see Supplemental Material). Next, all chemical structures that appear in Fig. 8 were evaluated computation-

**Table 3** Relative Gibbs free energy differences ( $\Delta G^*$ ) at 400 K in kcal/mol for monomeric complexes **3a** and **3b** (reactants) versus the ATRP  $k_{act}$ , CCT, and OMRP reaction products (**5a/5b**, **4a/4b**, and **6a/6b**, respectively).

Reaction Path	$\Delta G^*$ for $R = t$ -Bu	$\Delta G^*$ for $R=Et$	
ATRP $(3a/3b \rightarrow 5a/5b)$	1.9	-0.3	
CCT $(3a/3b \rightarrow 4a/4b)$	27.2	24.6	
OMRP $(3a/3b \rightarrow 6a/6b)$	11.9	13.0	

ally to determine the relative thermodynamics for the CCT, ATRP, and OMRP mechanisms; relative Gibbs free energy differences at 400 K ( $\Delta G^*$ ) are presented in Table 3. The free-radical fragment, PhCH<sub>3</sub>HC•, is used as a model for the growing polystyrene chain. The ATRP equilibrium products (5a/5b) are approximately the same Gibbs free energy at 400 K as reactants, suggesting ATRP of styrene will occur readily at 120 °C. The OMRP equilibrium products (6a/6b) are higher in Gibbs free energy at 400 K than reactants by approximately 12-13 kcal/mol. This suggests the OMRP mechanism may compete with ATRP yet will not sequester 3a/3b from the system to a large extent. Finally, the CCT equilibrium products are substantially higher in Gibbs free energy at 400 K with values of 27.2 kcal/mol for 4a (R = t-Bu) and 24.6 kcal/mol for 4b(R = Et). This data implies that CCT will compete more effectively with ATRP using the ethyl substituted catalyst 2 than for the tbutyl substituted catalyst 1, though the higher relative energy of the CCT equilibrium products also suggests CCT will be a lesser contributor than ATRP (or OMRP) for either catalyst. In summary, this analysis reflects the relative ground state energies of ATRP, CCT, and OMRP reactants and products in the equilibria that define each mechanism as presented in Fig. 8. The thermodynamic treatment presented here may help account for our experimental polymerization data for styrene at 120 °C with evidence for both ATRP and CCT pathways at this elevated temperature.

Fig. 8. Competing mechanistic equilibria for CCT ( $3a/3b \rightarrow 4a/4b$ ), ATRP ( $3a/3b \rightarrow 5a/5b$ ), and OMRP ( $3a/3b \rightarrow 6a/6b$ ). Compound numbers labeled "a" have R = t-Bu and compounds numbers labeled "b" have R = Et.

#### 3. Conclusions

Reported herein are two new iron amino pyridine complexes with a novel modification to the amino carbon. This study demonstrates the utility of these amino-pyridine iron(II) complexes for controlled radical polymerization. Subtle variation in the aminocarbon substituent from ethyl to t-butyl increases the observed rate of styrene polymerization. We propose that catalyst 1 displays a higher observed polymerization rate than catalyst 2 due to enhanced electron donation from its t-butyl amino carbon substituent and its smaller N<sub>pyr</sub>-Fe-N<sub>amine</sub> bite angle that are both compatible with the requisite Fe(III) complex on the left side of the ATRP propagation equilibrium (Fig. 1). Polymer characterization data including end group analysis suggests ATRP and CCT act as competing polymerization mechanisms for catalysts 1 and 2 under the conditions evaluated here. The elevated polymerization temperatures in this study may increase the prevalence of CCT as a competing pathway, however the  $k_{obs}$  values for styrene polymerization indicate these examples of amino-pyridine iron(II) catalysts may be less practical under lower temperature conditions. Work is underway to optimize the electronic features of new ligands for iron ATRP catalysts using computational thermodynamic ground state energies for ATRP and CCT equilibria to aid in catalyst design.

#### 4. Experimental section

#### 4.1. General considerations

All chemical reactions were carried out under an atmosphere of argon using standard Schlenk techniques unless otherwise noted. Argon gas was purified by passage over Drierite<sup>TM</sup>. All chemicals were purchased from Sigma Aldrich and used as received unless otherwise noted. Chloroform-d, benzene- $d_6$  and acetonitrile $d_3$  were purchased from Sigma Aldrich and dried over molecular sieves (8-12 mesh, 4 Å, activated) before use. An MBraun Manual Solvent Purification System (MB-SPS) was used to obtain the following anhydrous solvents: toluene, pentane, dichloromethane, acetonitrile, tetrahydrofuran, diethyl ether; when used in a glove box, solvents were submitted to three freeze-pump-thaw cycles before use. Anhydrous tetrahydrofuran for all purposes was additionally dried over molecular sieves (8-12 mesh, 4 Å, activated) before use. Anhydrous diethyl ether used in ligand synthesis (LiAlH<sub>4</sub> reduction reactions) was purchased from J.T. Baker in 250 mL bottles, and a fresh bottle was used for each synthetic trial. Molecular sieves (8-12 Mesh, 4 Å) were purchased from J.T. Baker and activated before use. Silica gel used for flash chromatography was purchased from Aldrich (200-425 mesh) [53]. n-BuLi was purchased from Sigma Aldrich as a 1.6 M solution in hexanes (Sure/Seal bottle<sup>TM</sup>). Iron(II) dichloride (99.9%, Sigma Aldrich) was complexed with anhydrous THF to give FeCl<sub>2</sub>(THF)<sub>1.5</sub> using reported procedures [54]. Ligand **A**,  $[2-[(2,6-Me_2-C_6H_3)NHCH(t-Bu)]C_5H_4N]$ , and Ligand **B**,  $2-\{(2,6-Me_2-C_6H_3)NC(Et)\}C_5H_4N$ , were prepared as described previously [19].

#### 4.2. Characterization

NMR spectra were recorded on a Varian Mercury 300 Plus spectrometer at 300 MHz ( $^{1}$ H) and 75 MHz ( $^{13}$ C) at 293 K and JEOL 400 MHz spectrometer at 400 MHz ( $^{1}$ H); all chemical shifts were referenced relative to the NMR solvent (either residual protio or  $^{13}$ C signals for the solvent peak(s)). The following abbreviations are used for NMR splitting patterns: pt (pseudo triplet) and br s (broad singlet). A stock solution of acetonitrile- $d_3$ : anhydrous dichloromethane: anhydrous THF (1:2:7, v/v) was used for Evans' NMR magnetic susceptibility measurements [42,55-56] for complexes **1** and **2**. Five different concentrations were tested for

each complex and average  $\mu_{\rm eff}$  values are reported. Infrared spectra were recorded using a Perkin-Elmer Spectrum One FTIR System; samples were prepared by placing the compounds on a diamond attenuated total reflectance (ATR) plate in either solid or liquid form. Elemental analyses were performed at Atlantic Microlab, Inc. in Norcross, Georgia.

#### 4.3. Crystallography

A single crystal was mounted using NVH immersion oil onto a plastic fiber and run at a data collection temperature of 100 K. Data were collected on a Brüker-AXS Kappa APEX II CCD diffractometer with 0.71073 Å MoK $\alpha$  radiation. Unit cell parameters were obtained from 60 data frames,  $0.5^{\circ}$   $\Phi$ , from three different sections of the Ewald sphere. The data set was treated with SADABS absorption corrections based on redundant multi-scan data. Structures were solved by direct methods using XL or XT and refined by full-matrix least-squares on  $F^2$  using XL interfaced through APEX2 or OLEX2. All non-hydrogen atoms were refined with anisotropic displacement parameters. All hydrogen atoms were treated as idealized contribution. Details of the refinements for each structure are as follows: Complex 1: Refinement proceeded normally with one half of the inversion related dimer per asymmetric unit. Complex 2: Refinement proceeded normally with one half of the inversion related dimer per asymmetric unit. Crystal data and structure refinement details for complexes 1 and 2 appear in Table 4.

#### 4.4. Computational studies

All calculations were performed using Gaussian09 Rev. D.01 [57]. All structures were optimized in the gas-phase at the unrestricted M06-L level of theory using the Opt=Tight keyword. The 6-31G\*\* basis set was used for all main group elements and the SDD basis set was used for Fe, with the first 10 electrons represented by an effective core potential. All stationary points were determined to be minima (no imaginary frequencies) through vibrational analysis. Harmonic frequencies were calculated from analytic second derivatives of the energy with respect to nuclear coordinates. All DFT calculations utilized a finer grid for integration using the Integral=UltraFine option.

Determination of more reliable reaction energies was achieved by performing additional calculations at the previously mentioned optimized geometries. This was accomplished by performing single point energy calculations with a larger basis set and inclusion of solvent effects. Gibbs free energies were determined for each species and are the sum of four terms:  $E_0$ ,  $G_{solv}$ ,  $G_{corr}$ , and  $G^{0\to *}$ . E<sub>0</sub> is the electronic energy, G<sub>solv</sub> is the Gibbs free energy of solvation, G<sub>corr</sub> is the thermal correction to the Gibbs free energy, and  $G^{0\to *}$  is the correction required in going from the standard state in the gas phase (1 atm) to solution phase (1 M).  $G^{0\rightarrow *}$  is a fixed value at a given temperature and was determined to be 2.8 kcal/mol at 400 K (close to experimental polymerization temperature). G<sub>corr</sub> was calculated at 400 K as well, using the structural and vibrational quantities determined from the gas-phase geometry optimizations. The electronic energies and Gibbs free energies of solvation were calculated at the M06-L level of theory using the SMD solvation model, with toluene as the chosen solvent. The 6-311+G(2d,p) basis set was used for main group atoms and the all-electron def2TZVP basis set for Fe. In this approach, the value of G<sub>solv</sub> does not include the effect of geometry relaxation due to solvent.

#### 4.5. Polymerization

Styrene was purchased from Sigma Aldrich, and before use inhibitor was removed by passing through a bed of aluminum ox-

Table 4 Crystal data and structure refinement for complexes  ${\bf 1}$  and  ${\bf 2}$ .

	1	2
Empirical formula	$C_{18}H_{24}Cl_2FeN_2$	C <sub>16</sub> H <sub>20</sub> Cl <sub>2</sub> FeN <sub>2</sub>
Formula weight	395.14	367.09
Temperature	100 K	100 K
Crystal system	Monoclinic	Orthorhombic
Space group	P2 <sub>1</sub> /c	Pbca
Unit cell dimensions	$a=8.89400(10)$ Å; $\alpha = 90^{\circ} b=15.0669(2)$ Å; $\beta=105.0390(10)^{\circ}$	$a=15.231(3)$ Å; $\alpha = 90$ ° $b=13.717(3)$ Å; $\beta = 90$ ° $c=16.404(3)$ Å;
	$c=14.2424(2) \text{ Å; } \gamma = 90^{\circ}$	$\gamma = 90^{\circ}$
Volume	1843.18(4) Å <sup>3</sup>	3427.2(13) Å <sup>3</sup>
Z	4	8
Density (calculated)	$1.428 \text{ Mg/m}^3$	1.423 Mg/m <sup>3</sup>
Absorption coefficient	1.108 mm <sup>-1</sup>	1.186 mm <sup>-1</sup>
F(000)	828	1520
Crystal size	$0.3 \times 0.25 \times 0.2 \text{ mm}^3$	$0.25 \times 0.25 \times 0.13 \text{ mm}^3$
Theta range for data collection	2.005 to 34.338°	4.704 to 72.628°
Index ranges	-14 <= h <= 14, -23 <= k <= 23, -22 <= l <= 22	$-25 \le h \le 25, -22 \le k \le 22, -27 \le l \le 27$
Reflections collected	76,550	74,577
Independent reflections	7710 [ $R(int) = 0.0275$ , $R(sigma) = 0.0134$ ]	8307 $[R(int) = 0.0612, R(sigma) = 0.0316]$
Data / restraints / parameters	7710 / 0 / 216	11,384 / 1 / 385
Goodness-of-fit on F <sup>2</sup>	1.035	1.031
Final $R$ indices $[I>2\text{sigma}(I)]$	$R_1 = 0.0221$ , $wR_2 = 0.0563$	$R_1 = 0.0326$ , w $R_2 = 0.0784$
R indices (all data)	$R_1 = 0.0264$ , $wR_2 = 0.0590$	$R_1 = 0.0476$ , $wR_2 = 0.0869$
Largest diff. peak and hole	0.577 and -0.258 e · Å <sup>-3</sup>	0.78 and -0.29 e · Å <sup>-3</sup>

ide (activated, basic), subjected to two freeze/pump thaw cycles, and then bubbled with argon for 2 h. 1-phenylethyl chloride (±1-chloroethyl benzene, 1-PECl) initiator was purchased from Sigma Aldrich and used as received for polymerization trials with catalyst 1. 1-phenylethyl chloride was synthesized as described elsewhere [58] and used for polymerization trials with catalyst 2. Hydrochloric acid and methanol used for polymerization quenching were purchased from Fisher Scientific.

#### 4.6. Syntheses

#### 4.6.1. Preparation of $[2-[(2,6-Me_2-C_6H_3)NHCH(Et)]C_5H_4N]$ , ligand **C**

Lithium aluminum hydride (0.54 g, 14 mmol, 2.5 equiv) was weighed into an oven dried, 50 mL 2-neck round bottom flask that had been purged with argon. Anhydrous diethyl ether (4 mL) was added to the reaction flask dropwise via syringe and the mixture stirred to yield a slurry. Ligand B (1.4 g, 5.9 mmol, 1.0 equiv) was dissolved in anhydrous diethyl ether (6 mL) and this solution was added dropwise to the reaction flask containing the LiAlH<sub>4</sub> slurry. The reaction mixture was stirred at 22 °C for 23 h. To quench excess LiAlH<sub>4</sub>, the reaction flask was cooled to 0 °C with an ice-water bath. An aliquot of cold anhydrous diethyl ether (11 mL) was added to the reaction flask, followed by cautious, dropwise addition of alternating aliquots of distilled water (4 × 0.25 mL) and diethyl ether (4 × 1 mL) with a 10-minute wait between each aliquot. After the final water and diethyl ether addition the reaction mixture was a yellow solution with suspended white solid. Cold ethyl acetate (3 mL) was added to assure quenching was complete and to help extract the desired product. The reaction mixture was stirred at 22 °C for 30 min, and then filtered through a bed of Celite and washed with diethyl ether (50 mL). This filtrate was washed with saturated aqueous sodium chloride (1 × 10 mL) and dried with sodium sulfate before removal of solvent in vacuo to yield a yellow oil. The crude product was purified via flash silica gel chromatography using 15% ethyl acetate, 1% triethyl amine – hexanes (v/v/v)and dried in vacuo to give a yellow oil. Final purification was completed by adding 10 mL pentane to the aforementioned yellow oil, filtering through a pipet fitted with a Kimwipe to remove final solid impurities and the filtrate dried in vacuo to yield the final product as a yellow oil (0.81 g, 60% yield). (Found: C 79.90, H 8.44, N 11.49%. Calculated for  $C_{16}H_{20}N_2$ : C 79.96, H 8.39, N 11.66%.  $v_{max}$ (ATR)/cm $^{-1}$ : 3362 (N-H). <sup>1</sup>H NMR (300 MHz, benzene- $d_6$ , 22  $^{\circ}$ C)  $\delta$ /ppm: 0.73 (3H, t, CH<sub>2</sub>CH<sub>3</sub>), 1.962 (2H, q, J = 7.0 Hz, CH<sub>2</sub>CH<sub>3</sub>), 2.19 (6H, s, CH<sub>3</sub>), 4.14 (1H, t, J = 6.4 Hz, CH), 4.37 (1H, br s, NH), 6.52 - 6.88 (6H, multiplets, Ar, py), 8.40 (1H, dd, J = 4.4 Hz, 1.5 Hz,  $H_f$ ).  $^{13}$ C NMR (75 MHz, chloroform-d, 22 $^{\circ}$  C)  $\delta$ /ppm: 10.57 (CH<sub>2</sub>CH<sub>3</sub>), 18.92 (CH<sub>2</sub>CH<sub>3</sub>), 29.17 (CH<sub>3</sub>), 63.70 (CHNH), 121.16, 121.62, 122.35, 135.33, 145.34, 149.48, 162.49 (aromatics).

## 4.6.2. Preparation of ( $[2-[(2,6-Me_2-C_6H_3)NHCH(t-Bu)]C_5H_4N]$ FeCl<sub>2</sub>)<sub>2</sub>, **1**

Under an atmosphere of nitrogen in an MBraun Unilab glovebox, a slurry of FeCl<sub>2</sub>(THF)<sub>15</sub> (0.42 g, 1.8 mmol, 1.0 equiv) in toluene (10 mL) was prepared in an oven dried 50 mL round bottom flask. To prepare ligand A for transfer into the glovebox, the appropriate amount was dissolved in anhydrous dichloromethane, transferred to a round bottom flask with 180° vacuum adapter, and then concentrated to dryness in vacuo. Inside the glove box, ligand A (0.53 g, 2.0 mmol, 1.1 equiv) was dissolved in toluene (3 mL) and this solution was added dropwise via pipet to the FeCl<sub>2</sub>(THF)<sub>1.5</sub> slurry to yield a tan slurry. The solution was removed from the glovebox and heated in an oil bath with stirring under a flow of argon to 80 °C for 18 h, then the heat was increased to 100 °C for 23 h. The final reaction mixture was a brown solution with tan solids. After two freeze/pump/thaw cycles using a dry ice/acetone bath (-78 °C) the product mixture was returned to the glove box and pale tan solids were isolated via vacuum filtration. The crude product was further washed with diethyl ether and dried in vacuo to give a tan microcrystalline solid (0.71 g). (Found: C 47.62, H 5.47 N 6.02%. Calculated for C<sub>18</sub>H<sub>24</sub>N<sub>2</sub>FeCl<sub>2</sub>: C 54.71, H 6.12, N 7.09%. Consistent with the formula:  $C_{36}H_{48}N_4Fe_2Cl_4$  · 1.95 CH<sub>2</sub>Cl<sub>2</sub>. Recalculated: C 47.68, H 5.47, N 5.86%). Based on: C<sub>36</sub>H<sub>48</sub>N<sub>4</sub>Fe<sub>2</sub>Cl<sub>4</sub> · 1.95 CH<sub>2</sub>Cl<sub>2</sub> 87% yield of complex 1 was obtained.  $v_{max}$  (ATR)/cm<sup>-1</sup>: 3340 (N-H).  $\mu_{eff} = 5.71$  B M. (Evans' NMR method). Single crystals of complex **1** suitable for X-ray diffraction were obtained from cooling of a saturated solution of complex **1** in anhydrous acetonitrile at -28 °C over the course of 6 weeks.

4.6.3. Preparation of  $([2-[(2,6-Me_2-C_6H_3)NHCH(Et)]C_5H_4N]FeCl_2)_2$ , **2** Under an atmosphere of nitrogen in an MBraun Unilab glovebox, a slurry of FeCl<sub>2</sub>(THF)<sub>1.5</sub> (0.48 g, 2.0 mmol, 1.0 equiv) in toluene (20 mL) was prepared in an oven dried 50 mL round bottom flask. To prepare ligand C for transfer into the glovebox, the appropriate amount was dissolved in anhydrous dichloromethane, transferred to a round bottom flask with 180° vacuum adapter, and then concentrated to dryness in vacuo. Inside the glove box, ligand C (0.59 g, 2.5 mmol, 1.2 equiv) was dissolved in toluene (3 mL) and this solution was added dropwise via pipet to the FeCl<sub>2</sub>(THF)<sub>1.5</sub> slurry to yield a tan slurry. The solution was removed from the glovebox and heated in an oil bath with stirring under a flow of argon to 80  $^{\circ}\text{C}$  for 21 h. The reaction was removed from heat and allowed to cool to 22 °C. The final reaction mixture was a golden colored solution with brown solids. After two freeze/pump/thaw cycles using a dry ice/acetone bath (-78 °C) the product mixture was returned to the glove box where tan solids were isolated via vacuum filtration. The crude product was further washed with diethyl ether and dried in vacuo to give a tan microcrystalline solid (0.64 g). (Found: C 50.69, H 5.42, N 7.10%. Calculated for C<sub>16</sub>H<sub>20</sub>N<sub>2</sub>FeCl<sub>2</sub>: C 52.35, H 5.49, N 7.63%. Consistent with the formula: C<sub>16</sub>H<sub>20</sub>N<sub>2</sub>FeCl<sub>2</sub> · 0.20 CH<sub>2</sub>Cl<sub>2</sub>. Recalculated: C 50.66, H 5.35, N 7.29%). Based on: C<sub>16</sub>H<sub>24</sub>N<sub>2</sub>FeCl<sub>2</sub> · 0.20 CH<sub>2</sub>Cl<sub>2</sub>. 83% yield of compound 2 was obtained. MS (ESI, m/z): [M-Cl]<sup>+</sup> 697.1017; [L+H]+ 241.1481.  $v_{max}$ 

(ATR)/cm $^{-1}$ : 3326 (N-H stretch).  $\mu_{eff}=5.51$  B M. (Evans' NMR method). Single crystals of complex **2** suitable for X-ray diffraction were obtained from vapor diffusion of pentane into dichloromethane at 25 °C over the course of 2 days.

#### 4.7. General procedure for styrene polymerization

Polymerizations were conducted in bulk under an inert atmosphere using 1-phenylethyl chloride as initiator and a polymerization temperature of 120 °C. All glassware was oven dried overnight before use. Inhibitor-free, degassed styrene was stored in a refrigerator for no more than 12 h before use. A minimal amount of oxygen may diffuse into the septum-capped vial of styrene during storage despite attempts to exclude it, potentially contributing to an induction time for the polymerization trials described here. Under an atmosphere of nitrogen in an MBraun Unilab glovebox. the metal complex of interest (1 or 2) was weighed into a 20 mL scintillation vial containing a stir bar, topped with a septum cap, and then removed from the glovebox. Ratios of [styrene]:[Fe]:[1phenylethyl chloride] were 300: 1.0: 1.0 for each polymerization trial reported in Figs. 5 and 6 and Table 2. All reactions were normalized to 8 mL styrene. Styrene was added to the reaction vial via syringe, followed by 1-phenylethyl chloride initiator. Masses of styrene and initiator dispensed were confirmed by back-weighing the syringes. The reaction vial was then placed in an aluminum heating block on a hot plate. The hot plate temperature was controlled by a thermocouple placed in the aluminum block connected to a temperature controller built in-house. Immediately after adding initiator to the vial, stirring and heat commenced. The polymerization mixture is estimated to reach reaction temperature between 5 and 10 min based on independent tests. Polymerization progress was monitored by removing 0.2 mL aliquots from the reaction mixture via syringe at 1, 2, 4, 6, 8, 10 and 11 hour intervals for catalyst 1 and 2, 3, 4, 6, 8, and 10 hour intervals for catalyst 2. The first 0.1 mL of the aliquot was used to determine percent monomer conversion by <sup>1</sup>H NMR measurement; polymerization

was halted by passing this 0.1 mL of solution over a bed of basic alumina to remove the iron complex, then rinsing the solid support using chloroform-d. Monomer conversion was determined by integration of styrene  $\mathbf{H}_2C=C\mathbf{HPh}$  peaks (integration range 5.2–5.4 ppm and 5.7–6.0 ppm) relative to aromatic polystyrene (CH $\mathbf{PhCH}_2$ )<sub>n</sub> and styrene  $\mathbf{H}_2C=C\mathbf{HPh}$  peaks (integration range 6.35–6.95 ppm). The second 0.1 mL of the aliquot was quenched by adding it dropwise to 1 mL THF to later recover as polymer. Precipitating the polymer from the combined THF solution and  $^1\mathbf{H}$  NMR sample was accomplished by dropwise addition of both into 30 mL of 5% acidified methanol solution (HCl:CH<sub>3</sub>OH, v/v) with strong mixing to give suspended white solid polymer particles. Solid polymer was isolated from the acidified methanol by vacuum filtration using a glass fritted funnel and washed with methanol. Polymer was dried for 10 h in a vacuum oven at 80  $^{\circ}$ C.

#### 4.8. Polystyrene GPC analysis

At least 24 h prior to analysis, GPC samples were prepared by weighing approximately 5 mg of polymer into a 3-dram vial and diluting to a concentration of 2 mg/mL with HPLC grade THF. Polymer solutions were then filtered into 1.5 mL vials using 4 mm, 0.45 µM Teflon syringe filters purchased from National Scientific. For all GPC analysis, THF was used as a mobile phase with a flow rate of 1 mL min<sup>-1</sup>. GPC analyses for samples from Table 3, entries 1-4 were conducted at Temple University using instrument 1: Shimadzu instrument fitted with three Polymer Laboratories columns in series: PolarGel-M (300  $\times$  7.5 mm) with 8  $\mu$ m particle size, and UV-Vis detector monitoring at 254 nm. GPC analyses for samples from Table 3, entries 5-7 were conducted at Drexel University using instrument 2: a Shimadzu instrument fitted with a PLgel 5 μm mixed Agilent Technologies column followed in series with a PLgel 5 µm 50 Å Agilent Technologies column, and UV-Vis detector monitoring at 254 nm. Sample molecular weight  $(M_n)$  and dispersity (D) were determined from a calibration curve created using polystyrene standards (Polymer Laboratories, EasiCal PS-1).

#### **Declaration of Competing Interest**

The authors declare that they have no known competing financial interests or personal relationships that could have appeared to influence the work reported in this paper.

#### Acknowledgements

We acknowledge Danielle M. Lovett for the preparation of ligand **B** and Brad Thorstensen for the construction of the polymerization temperature controller. We thank Dr. Graham Dobereiner and Dr. Evan Samples (Temple University) and Dr. Masoud Soroush and Pat Corcoran (Drexel University) for use of their GPC instrumentation, and we thank Dr. Walter Boyko for assistance with NMR spectroscopy. Financial support from the Villanova University College of Liberal Arts and Sciences – Graduate Student Summer Research Fellowship (LMT and SEJ), the Villanova Undergraduate Research Fellows Program (VS and MRD), and the Villanova University Department of Chemistry and College of Liberal Arts and Sciences is gratefully acknowledged. This work was funded by a Major Research Instrumentation grant from the National Science Foundation (CHE-1827930).

#### Supplementary materials

Supplementary material associated with this article can be found, in the online version, at doi:10.1016/j.jorganchem.2020. 121456.

#### References

- S.R. Tamang, M. Findlater, Emergence and Applications of Base Metals (Fe, Co, and Ni) in Hydroboration and Hydrosilylation, Molecules 24 (2019) 3194.
- [2] B. Bruin, P. Gualco, N.D. Paul, Redox Non-Innocent Ligands Reactivity and Catalysis Redox Non-Innocent Ligands: Reactivity and Catalysis, in: Ligand Des. Met. Chem., Wiley-Blackwell, 2016, pp. 176–204.
- [3] M.C. White, Base-Metal Catalysis: Embrace the Wild Side, Adv. Synth. Catal. 358 (2016) 2364–2365.
- [4] M. Albrecht, R. Bedford, B. Plietker, Catalytic and Organometallic Chemistry of Earth-Abundant Metals, Organometallics 33 (2014) 5619–5621.
- [5] K. Matyjaszewski, J. Xia, Atom Transfer Radical Polymerization, Chem. Rev. 101 (2001) 2921–2990.
- [6] K. Matyjaszewski, Atom Transfer Radical Polymerization (ATRP): Current Status and Future Perspectives, Macromolecules 45 (2012) 4015–4039.
   [7] K. Matyjaszewski, N.V. Tsarevsky, Macromolecular Engineering by Atom Trans-
- K. Matyjaszewski, N.V. Tsarevsky, Macromolecular Engineering by Atom Transfer Radical Polymerization, J. Am. Chem. Soc. 136 (2014) 6513–6533.
- [8] P.L. Golas, L.A. Mueller, K. Matyjaszewski, Atom Transfer Radical Polymerization, in: Encycl. Polym. Sci. Technol, 1, 4th Ed., John Wiley & Sons, Inc., 2014, pp. 720–745.
- [9] K. Matyjaszewski, Advanced Materials by Atom Transfer Radical Polymerization, Adv. Mater 30 (2018) 1706441.
- [10] M. Kamigaito, T. Ando, M. Sawamoto, Metal-Catalyzed Living Radical Polymerization, Chem. Rev 101 (2001) 3689–3746.
- [11] M. Ouchi, T. Terashima, M. Sawamoto, Precision Control of Radical Polymerization via Transition Metal Catalysis: From Dormant Species to Designed Catalysts for Precision Functional Polymers, Acc. Chem. Res. 41 (2008) 1120–1132.
- [12] M. Ouchi, T. Terashima, M. Sawamoto, Transition Metal-Catalyzed Living Radical Polymerization: Toward Perfection in Catalysis and Precision Polymer Synthesis, Chem. Rev. 109 (2009) 4963–5050.
- [13] M. Ouchi, M. Sawamoto, 50th Anniversary Perspective: Metal-Catalyzed Living Radical Polymerization: Discovery and Perspective, Macromolecules 50 (2017) 2603–2614.
- [14] B.M. Rosen, V. Percec, Single-Electron Transfer and Single-Electron Transfer Degenerative Chain Transfer Living Radical Polymerization, Chem. Rev 109 (2009) 5069–5119.
- [15] J.-S. Wang, K. Matyjaszewski, Controlled/"living" Radical Polymerization. Atom Transfer Radical Polymerization in the Presence of Transition-Metal Complexes, J. Am. Chem. Soc. 117 (1995) 5614–5615.
- [16] M. Kato, M. Kamigaito, M. Sawamoto, T. Higashimura, Polymerization of Methyl Methacrylate with the Carbon Tetrachloride/Dichlorotris-(Triphenylphosphine)-Ruthenium(II)/Methylaluminum Bis(2,6-Di-Tert-Butylphenoxide) Initiating System: Possibility of Living Radical Polymerization, Macromolecules 28 (1995) 1721–1723.
- [17] R. Poli, M.P. Shaver, ATRP/OMRP/CCT Interplay in Styrene Polymerization Mediated by Iron (II) Complexes: A DFT Study of the α-Diimine System, Chem.-Eur. J 20 (2014) 17530–17540.
- [18] T.M. Smit, A.K. Tomov, G.J.P. Britovsek, V.C. Gibson, A.J.P. White, D.J. Williams, The effect of imine-carbon substituents in bis(imino)pyridine-based ethylene polymerisation catalysts across the transition series, Catal. Sci. Technol. 2 (2012) 643–655.
- [19] D.M. Lovett, L.M. Thierer, E.E.P. Santos, R.L. Hardie, W.G. Dougherty, N.A. Piro, W.S. Kassel, B.M. Cromer, E.B. Coughlin, D.L. Zubris, Structural Analysis of Imino- and Amino-Pyridine Ligands for Ni(II): Precatalysts for the Polymerization of Ethylene, J. Organomet. Chem. 863 (2018) 44–53.
- [20] S. Zai, H. Gao, Z. Huang, H. Hu, H. Wu, Q. Wu, Substituent Effects of Pyridine-Amine Nickel Catalyst Precursors on Ethylene Polymerization, ACS Catal. 2 (2012) 433–440.
- [21] S. Zai, F. Liu, H. Gao, C. Li, G. Zhou, S. Cheng, L. Guo, L. Zhang, F. Zhu, Q. Wu, Longstanding Living Polymerization of Ethylene: Substituent Effect on Bridging Carbon of 2-Pyridinemethanamine Nickel Catalysts, Chem. Commun. 46 (2010) 4321–4323.
- [22] Y.-C. Lin, K.-H. Yu, Y.-F. Lin, G.-H. Lee, Y. Wang, S.-T. Liu, J.-T. Chen, Synthesis, Structures of (Aminopyridine)Nickel Complexes and Their Use for Catalytic Ethylene Polymerization, Dalton Trans. 41 (2012) 6661–6670.
- [23] T. Ando, M. Kamigaito, M. Sawamoto, Iron(II) Chloride Complex for Living Radical Polymerization of Methyl Methacrylate, Macromolecules 30 (1997) 4507–4510
- [24] K. Matyjaszewski, M. Wei, J. Xia, N.E. McDermott, Controlled/"Living" Radical Polymerization of Styrene and Methyl Methacrylate Catalyzed by Iron Complexes, Macromolecules 30 (1997) 8161–8164.
- [25] Z. Xue, D. He, X. Xie, Iron-Catalyzed Atom Transfer Radical Polymerization, Polym. Chem. 6 (2015) 1660–1687.
- [26] R. Poli, L.E.N. Allan, M.P. Shaver, Iron-Mediated Reversible Deactivation Controlled Radical Polymerization, Prog. Polym. Sci. 39 (2014) 1827–1845.
- [27] D.F. Grishin, I.D. Grishin, Iron-Based Catalytic Systems in Atom-Transfer Controlled-Radical-Polymerization Processes, Polym. Sci. Ser. C 57 (2015) 32–64.
- [28] V.C. Gibson, R.K. O'Reilly, D.F. Wass, A.J.P. White, D.J. Williams, Iron Complexes Bearing Iminopyridine and Aminopyridine Ligands as Catalysts for Atom Transfer Radical Polymerisation, Dalton Trans. 14 (2003) 2824–2830.
- [29] V.C. Gibson, R.K. O'Reilly, W. Reed, D.F. Wass, A.J.P. White, D.J. Williams, Four-Coordinate Iron Complexes Bearing α-Diimine Ligands: Efficient Catalysts for Atom Transfer Radical Polymerisation (ATRP), Chem. Commun. 17 (2002) 1850–1851.
- [30] V.C. Gibson, R.K. O'Reilly, D.F. Wass, A.J.P. White, D.J. Williams, Polymerization of Methyl Methacrylate Using Four-Coordinate (α-Diimine)Iron Catalysts: Atom Transfer Radical Polymerization vs Catalytic Chain Transfer, Macromolecules 36 (2003) 2591–2593.

- [31] T.G. Ribelli, M. Fantin, J.-C. Daran, K.F. Augustine, R. Poli, K. Matyjaszewski, Synthesis and Characterization of the Most Active Copper ATRP Catalyst Based on Tris[(4-Dimethylaminopyridyl)Methyl]Amine, J. Am. Chem. Soc. 140 (2018) 1525–1534.
- [32] R.K. O'Reilly, V.C. Gibson, A.J. White, D.J. Williams, Design of Highly Active Iron-Based Catalysts for Atom Transfer Radical Polymerization: Tridentate Salicylaldiminato Ligands Affording near Ideal Nernstian Behavior, J. Am. Chem. Soc. 125 (2003) 8450-8451.
- [33] J. Louie, R.H. Grubbs, Highly Active Iron Imidazolylidene Catalysts for Atom Transfer Radical Polymerization, Chem. Commun. 16 (2000) 1479–1480.
   [34] L.E. Allan, J.P. MacDonald, G.S. Nichol, M.P. Shaver, Single Component Iron
- [34] L.E. Allan, J.P. MacDonald, G.S. Nichol, M.P. Shaver, Single Component Iron Catalysts for Atom Transfer and Organometallic Mediated Radical Polymerizations: Mechanistic Studies and Reaction Scope, Macromolecules 47 (2014) 1249–1257.
- [35] L.E. Allan, J.P. MacDonald, A.M. Reckling, C.M. Kozak, M.P. Shaver, Controlled Radical Polymerization Mediated by Amine-Bis (Phenolate) Iron (III) Complexes, Macromol. Rapid Commun. 33 (2012) 414–418.
- [36] E. Fazekas, G.S. Nichol, J.A. Garden, M.P. Shaver, Iron(III) Half Salen Catalysts for Atom Transfer Radical and Ring-Opening Polymerizations, ACS Omega 3 (2018) 16945–16953.
- [37] J. Raynaud, J.Y. Wu, T. Ritter, Iron-Catalyzed Polymerization of Isoprene and Other 1,3-Dienes, Angew. Chem. Int. Ed. 51 (2012) 11805–11808.
   [38] O.H. Hashmi, Y. Champouret, M. Visseaux, Highly Active Iminopyridyl
- [38] O.H. Hashmi, Y. Champouret, M. Visseaux, Highly Active Iminopyridyl Iron-Based Catalysts for the Polymerization of Isoprene, Molecules 24 (2019) 3024.
- [39] G. Zhu, X. Zhang, M. Zhao, L. Wang, C. Jing, P. Wang, X. Wang, Q. Wang, Influences of Fluorine Substituents on Iminopyridine Fe(II)- and Co(II)-Catalyzed Isoprene Polymerization, Polymers (Basel) 10 (2018) 934.
- [40] L. Guo, X. Jing, S. Xiong, W. Liu, Y. Liu, Z. Liu, C. Chen, Influences of Alkyl and Aryl Substituents on Iminopyridine Fe(II)- and Co(II)-Catalyzed Isoprene Polymerization, Polymers (Basel) 8 (2016) 389.
- [41] C. Jing, L. Wang, Q. Mahmood, M. Zhao, G. Zhu, X. Zhang, X. Wang, Q. Wang, Synthesis and Characterization of Aminopyridine Iron(II) Chloride Catalysts for Isoprene Polymerization: Sterically Controlled Monomer Enchainment, Dalton Trans. 48 (2019) 7862–7874.
- [42] D.F. Evans, The Determination of the Paramagnetic Susceptibility of Substances in Solution by Nuclear Magnetic Resonance, J. Chem. Soc. Chem. Commun. (1959) 2003–2005.
- [43] A.W. Addison, T.N. Rao, J. Reedijk, J. van Rijn, G.C. Verschoor, Synthesis, Structure, and Spectroscopic Properties of Copper (II) Compounds Containing Nitrogen–Sulphur Donor Ligands; the Crystal and Molecular Structure of Aqua [1,7-Bis(N-Methylbenzimidazol-2'-yl)-2,6-Dithiaheptane] Copper (II) Perchlorate, J. Chem. Soc. Dalton Trans. 7 (1984) 1349–1356.
- [44] L.E. Állan, M.P. Shaver, A.J. White, V.C. Gibson, Correlation of Metal Spin-State in  $\alpha$ -Diimine Iron Catalysts with Polymerization Mechanism, Inorg. Chem. 46 (2007) 8963–8970.
- [45] R. Poli, New Phenomena in Organometallic-Mediated Radical Polymerization (OMRP) and Perspectives for Control of Less Active Monomers, Chem.- Eur. J. 21 (2015) 6988-7001.
- [46] E. Le Grognec, J. Claverie, R. Poli, Radical Polymerization of Styrene Controlled by Half-Sandwich Mo(III)/Mo(IV) Couples: All Basic Mechanisms Are Possible, J. Am. Chem. Soc. 123 (2001) 9513–9524.
- [47] D.L. Coward, B.R.M. Lake, M.P. Shaver, Understanding Organometallic-Mediated Radical Polymerization with an Iron(II) Amine-Bis(Phenolate), Organometallics 36 (2017) 3322-3328.
- [48] C. Fliedel, R. Poli, Homolytically Weak Metal-Carbon Bonds Make Robust Controlled Radical Polymerizations Systems for "Less-Activated Monomers,", J. Organomet. Chem. 880 (2019) 241–252.
- [49] L. Thevenin, C. Fliedel, K. Matyjaszewski, R. Poli, Impact of Catalyzed Radical Termination (CRT) and Reductive Radical Termination (RRT) in Metal-Mediated Radical Polymerization Processes, Eur. J. Inorg. Chem. 42 (2019) 4489–4499.
- [50] Y. Nakamura, S. Yamago, Termination Mechanism in the Radical Polymerization of Methyl Methacrylate and Styrene Determined by the Reaction of Structurally Well-Defined Polymer End Radicals, Macromolecules 48 (2015) 6450-6456
- [51] Y. Wang, B. Li, F. Zhu, H. Gao, Q. Wu, Polymerization of Styrene Using Novel Bispyrazolylimine Dinickel (II)/Methylaluminoxane Catalytic Systems, J. Appl. Polym. Sci. 122 (2011) 545–550.
- [52] M.P. Shaver, L.E.N. Allan, H.S. Rzepa, V.C. Gibson, Correlation of Metal Spin State with Catalytic Reactivity: Polymerizations Mediated by  $\alpha$ -Diimine–Iron Complexes, Angew. Chem. Int. Ed. 45 (2006) 1241–1244.
- [53] W.C. Still, M. Kahn, A. Mitra, Rapid Chromatographic Technique for Preparative Separations with Moderate Resolution, J. Org. Chem. 43 (1978) 2923–2925.
- [54] M.T. Mock, C.V. Popescu, G.P. Yap, W.G. Dougherty, C.G. Riordan, Monovalent Iron in a Sulfur-Rich Environment, Inorg. Chem. 47 (2008) 1889–1891.
- [55] S.K. Sur, Measurement of Magnetic Susceptibility and Magnetic Moment of Paramagnetic Molecules in Solution by High-Field Fourier Transform NMR Spectroscopy, J. Magn. Reson. 82 (1989) 169–173.
- [56] E.M. Schubert, Utilizing the Evans Method with a Superconducting NMR Spectrometer in the Undergraduate Laboratory, J. Chem. Educ. 69 (1992) 62.
- [57] M.J. Frisch, G.W. Trucks, H.B. Schlegel, G.E. Scuseria, M.A. Robb, J.R. Cheeseman, G. Scalmani, V. Barone, B. Mennucci, G.A. Petersson, et al., Gaussian 09, Rev. D.01, Gaussian, Inc., Wallingford CT, 2013.
  [58] D. Landini, F. Rolla, Addition of Hydrohalogenic Acids to Alkenes in Aque-
- [58] D. Landini, F. Rolla, Addition of Hydrohalogenic Acids to Alkenes in Aqueous-Organic, Two-Phase Systems in the Presence of Catalytic Amounts of Onium Salts, J. Org. Chem. 45 (1980) 3527–3529.